

A Novel Interleaved DC-DC Converter with Reduced Loss for Fuel Cell Vehicle Application

M. Khalilzadeh*, B. Asaei^(C.A.) and M. R. Nikzad*

Abstract: In this paper a novel four-leg interleaved DC-DC boost converter is proposed which is well suitable for fuel cell vehicles (FCV) application. The voltage stress of two switches of this converter is half of the conventional interleaved converters. Therefore, smaller and cheaper switches can be utilized. Also "on" state duration of the two of four switches are reduced in comparison with conventional converter. Furthermore, comparing the losses of the proposed converter to conventional one – which is used in ‘Toyota Mirai 2015 – shows a significant loss reduction in full power range. The proposed converter is simulated within an FCV in urban and highway driving cycles using ADVISOR software. The results show that the average power loss of the converter is improved about 32% in urban cycle and about 17% in highway cycle comparing to conventional one.

Keywords: Fuel cell vehicle, Interleaved DC-DC converter, Converter loss calculation, Loss reduction, Toyota Mirai 2015.

I. Introduction

The demand for fossil fuel has increased in recent decades. One of the main reasons is the dramatically increase in personal vehicles produced each years which mainly powered by conventional internal combustion engines (ICEs). Due to the limitation of fossil fuel resources aside from the environmental aspects of using these kinds of fuels such as global warming, emissions released during combustion process and etc., electric vehicle (EVs) and FCVs are considered as attractive alternatives for ICEs.

In FCVs, unlike the conventional ICEs, the main power source is a fuel cell (FC) system. A battery pack is also used in order to generate the demanded peak power in vehicle drive cycles. Furthermore, during the start-up process of the fuel-cell the battery supplies the energy of the vehicle. A FC is generally supplied with hydrogen fuel and air [1]. Its output voltage is too low to supply the high-performance drive systems in vehicular power ratings [1, 2]. In fact, based on efficiency characteristic of the FC, even though it operates more efficient at lower temperatures, operation in high temperatures is inevitable because of the higher output voltage of the FC in this con-

dition [3]. Besides, this output voltage should be controlled and regulated at a desired voltage. Therefore, a step-up DC-DC converter should be adopted [4]-[6]. Utilizing this converter results in running the FC in lower temperature operating points which are more efficient. Among many different types of FCs, proton exchange membrane FCs (PEMFC) have the ability to operate at very low temperatures [3]. Owing to this feature and some other advantages they are almost the first candidate to be used in vehicular applications. Many topologies have been introduced in literature for DC-DC converter used in renewable energies such as FC applications [7]-[12].

The current ripple drawn from FC stacks has a major impact on its performance and durability [13, 14]. Therefore, the DC-DC converter which is used to regulate the DC-link voltage should have a proper input current characteristic. Converters proposed in [7]-[9] utilize coupled inductors and their input current ripple is relatively high. In [10]-[12] coupled inductors are used to increase the voltage conversion ratio in voltage multiplier cell. However, additional windings in high-power application not only complicates the design process, but also increase the overall power loss. Due to the low input current ripple, power splitting feature and high reliable operation of the interleaved converters, it is better to utilize these kinds of converters in high-power application. The reliability of these sorts of converters is discussed in [15]. Converters in [8, 9] and [12] are suitable for lower power demands.

In this paper a new DC-DC interleaved converter with a simple structure and reduced switch voltage stress is proposed. Low power dissipation, proper input current

Iranian Journal of Electrical & Electronic Engineering, 2017.

Paper received 16 August 2016 and accepted 8 April 2017.

* The authors are with the School of Electrical and Computer Engineering, University of Tehran, Tehran, Iran.

E-mails: m.khalilzadeh@ut.ac.ir, basaei@ut.ac.ir and nikzad@ut.ac.ir.

Corresponding Author: B. Asaei.

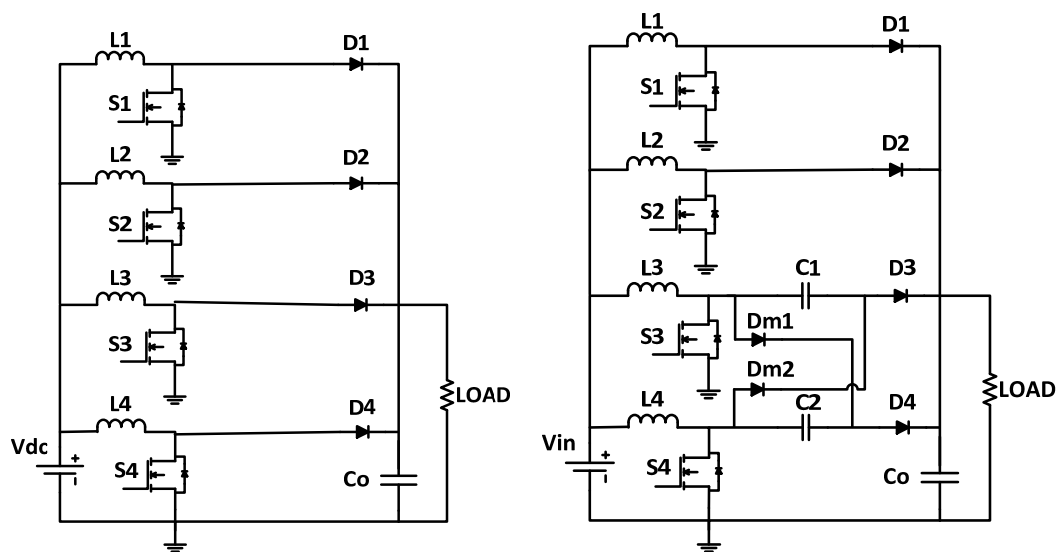


Fig.1. Circuit configuration of the (a) conventional interleaved converter used in Toyota Mirai 2015 (b) proposed converter

profile, simple and modular structure, make this converter a good candidate for high power applications.

2. Operation Principles of the Proposed Converter

Fig. 1(a) and Fig.1 (b) show the circuit configuration of a four-leg conventional interleaved DC-DC converter used in Toyota Mirai 2015 and the proposed converter, respectively. The proposed converter consists of a conventional two-leg (phase) interleaved boost converter combined with another interleaved converter with voltage multiplier cell. Two upper switches are driven similar to

a conventional two-leg interleaved converter with 50% phase shifted drive signals. Two lower switches are driven with 50% phase shifted signals with respect to each other in a way that the voltage gain of the upper and lower stages forced to be same. Hereafter, the operation of the lower side of the proposed converter will be further detailed. The upper side operation is the same as a conventional interleaved converter, so it is not discussed here. Circuit topology in each interval and the current-flow paths are illustrated in Fig. 2. Fig. 3 shows some of the typical key-waveforms of the proposed converter.

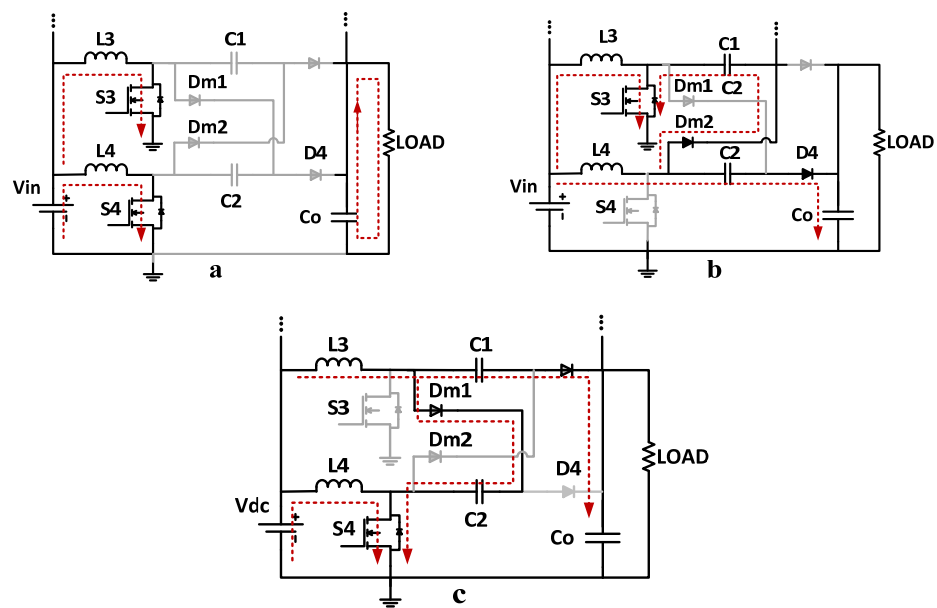


Fig. 2. Circuit topology and current paths in each operation interval (in the lower stage). (a) Interval 1&3, (b) Interval 2 (c) Interval 4

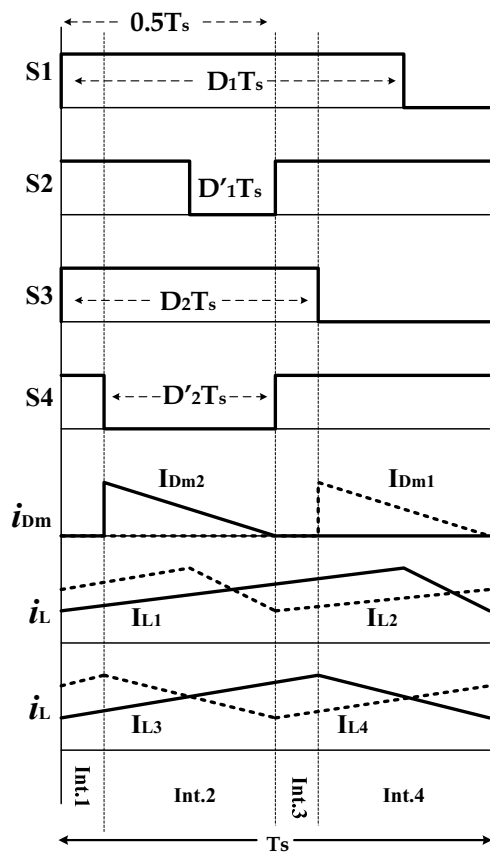


Fig. 3. The key waveforms of the proposed converter in CCM

Interval 1: In this mode of operation both of the lower switches (S3 & S4) are in "on" state. The input current splits between two inductors equally and energizes them. Output capacitor supplies the load power. This interval ends when S4 is turned into "off" state. Fig. 2(a) depicts the current-flow path of this mode of operation.

Interval 2: During this interval switch S3 is still on and S4 is in "off" state. Diode Dm2 and D4 are forward biased and are conducting the current. Therefore, C1 is energized and C2 is discharged into the output capacitor (Co). Furthermore, the current of inductor L3 is still increasing but inductor L4 is discharging its energy. As the same values are selected for the capacitors C1 and C2, the steady-state voltages of these capacitors are the same and equal to half of the output voltage of the converter. This mode of operation is lasted till S4 is off. Fig. 2(b) illustrates the circuit topology of interval 2 of the proposed converter.

Interval 3: This interval is similar to the interval 1, as shown in Fig. 2(a).

Interval 4: This interval is similar to interval 2 but unlike that, the switching condition of S3 and S4 are toggled. Therefore, L4 is in charging and L3 is in discharging mode. The circuit topology in this interval is depicted in

Fig. 2(c).

The voltage gain of the conventional stage is denoted in (1) as follows:

$$M_1 = \frac{V_o}{V_{in}} = \frac{1}{1 - D_1} \quad (1)$$

As mentioned before, the voltage of the capacitor C2 equals to half of the output voltage. Therefore, one can write the volt-second balance equation for inductor L4 in the switching period (Ts) as follows:

$$\langle V_{L4} \rangle_{T_s} = T_s \left(D_2 V_{in} + D_2' (V_{in} - V_o - \frac{V_o}{2}) \right) \quad (2)$$

Considering in (2), the voltage gain of the lower stage can be calculated as:

$$M_2 = \frac{V_o}{V_{in}} = \frac{2}{1 - D_2} \quad (3)$$

The input and output voltages of each stage are the same as the other stage. So the voltage gains should be same too. Therefore, results in:

$$D_1 = \frac{D_2 + 1}{2} \quad (4)$$

Equation (4) is used in controlling of the proposed topology in order to generate the switching commands. The steady-state "off" state voltage of the two lower switches is given in Eq. (5). As mentioned before, this voltage is half of the voltage of the switches of a conventional boost converter, resulting in lower loss and lower price in the proposed converter.

$$V_{S3\&S4} = \frac{V_o}{2} \quad (5)$$

In order to calculate the losses of the proposed converter and compare them with conventional interleaved boost converter, Eq. (6) and (7) are used [16, 17] where (6) denotes the losses related to switches (IGBTs) and (7) indicates the losses of diodes. These formulas include switching loss and conduction loss.

$$P_{Loss}^{IGBT} = U_{ceo} J_{c,avg} + r_c I_{c,RMS}^2 + (E_{on}^{IGBT} + E_{off}^{IGBT} + E_{rr}) f_s \quad (6)$$

Table 1. Vehicle specifications and driving conditions

Parameter	Value
Vehicle mass	1600 kg
Vehicle dimensions (length-width-height)	2349-1815-1535 mm
Vehicle Top speed	150 km/h
Vehicle acceleration time (0-96.6 km/h)	13 s
Gradeability	10% @ 100km/h
Aerodynamic drag coefficient	0.3
Wheel radius	290 mm
Rolling resistance coefficient	0.009
Air density	1.2 kg/m ³
Motor efficiency	94%
Transmission efficiency	90%

$$P_{Loss}^{Diode} = P_C + P_{rr} = U_{D,on} I_{D,avg} + r_D I_{D,RMS}^2 + E_{rr} f_s \quad (7)$$

In (6) U_{ce0} is IGBT "on" state zero-current collector-emitter voltage, r_c is collector emitter "on" state resistance, and E_{on} and E_{off} are turn-on and turn-off energy losses of the IGBT and E_{rr} is the parallel diode of IGBT reverse recovery energy loss. These values are extracted from the datasheet of the IGBT based on its operating point. Furthermore, $I_{c,avg}$ and $I_{c,RMS}$ are the collector average and RMS conducting current, respectively.

In (7), P_C denotes the diode conduction loss and P_{rr} is its reverse recovery loss. $U_{D,on}$, r_D and E_{rr} are diode forward voltage drop, on-state resistance and reverse recovery energy loss that can be extracted from the diode datasheet considering its operation point. $I_{D,avg}$, $I_{D,RMS}$ and f_s are the diode average and RMS conducting current and switching frequency, respectively.

As mentioned in [18], a conventional interleaved boost converter is used in some FCVs such as TOYOTA MIRAI 2015. But in order to reduce the converter losses, a specific strategy called "Efficient Phase Drive Control (EPDC)" is used in which in low demanding power, only one leg (phase) of the converter conducts and by increasing the load power the current will pass through the other legs (phases) one after another proportional to the load. Same strategy will be used for driving the proposed converter to maximize its efficiency. This strategy also guarantees that the converter operates in continuous conduction mode (CCM) in wide range of output load.

3. Design and Simulation Results of the Proposed Converter

In this section, the design and simulation results of the proposed converter are given. First, the converter is designed for an FCV. The vehicle parameters and driving conditions are given in Table 1. Then, the designed converter is simulated alone connecting to a variable load. In this stage the open-loop and close-loop responses are in-

vestigated. Finally the converter is tested in driving cycles along with the FCV in order to compare its losses with a conventional interleaved converter which operates in the same cycles.

Based on driving performance given in Table 1, sizing of the electric motor/generator, FC system and battery pack are required. It should be noted that the FC almost supplies the average output power and the dynamic power demand is handled by the battery pack. The electric motor should be designed based on the maximum demanded power of the vehicle. Therefore, (8) is used to calculate the maximum vehicle traction effort. Where F_t and F_w are forces corresponding with vehicle gradeability and weight respectively. Using (9) one can calculate the continuous output power of the electric motor/generator. v is the vehicle speed in which the corresponding force is calculated and η_{trans} is the transmission efficiency.

$$F_t = \max(F_{grade}, F_w) \quad (8)$$

$$P_{m/g} = \frac{F_t v}{\eta_{trans}} \quad (9)$$

In order to size the electric motor properly, the instantaneous vehicle demanded power should also be calculated which corresponds to its acceleration from one speed to another (Commonly zero speed to 96.6 km/h). Related equations are given in [19].

Considering vehicle and driving requirements given in Table 1 and pre-mentioned design procedure, an induction motor with the maximum power of 75 kW is chosen. Furthermore, a 55 kW FC system and 40 kW battery pack are selected which their details are given in Table 2. Hence, a 60kW uni-directional DC-DC converter is needed for the selected FC system. For that purpose the proposed four-leg topology is utilized. Parameters of the converter are given in Table 2. Hereafter the performance of the proposed converter is investigated under various computer

Table 1. Vehicle specifications and driving conditions

Parameter	Value / Type
Converter max. power	60 kW
DC link voltage	650 V
Motor/Gen. max. power	75 kW – Ind. motor
Motor/Gen. efficiency	94%
Fuel cell nominal power	55 kW– PEM
Fuel cell nominal out. voltage	144 V
Battery pack max. out. power	40 kW – Ni-MH
Vehicle total mass	1600 kg
S1 & S2 IGBTs	FF150R12KS4 - 1200V 150A
S3 & S3 IGBTs	BSM150GB60DLC–600V 150A
D3 & D4 Diodes	RURU15060 – 600V 150A
D1 & D2 & Dm diodes	S4380 – 800V 150A
C1 & C2 Capacitors	100 uF
L1 & L2 Inductance value	400 uH
L3 & L4 Inductance value	300 uH
Switching frequency	10 kHz

simulations in order to verify theoretical analysis and design procedure.

3. 1. Simulation of the converter alone

Matlab SIMULINK software is chosen for simulation. The data of the converter elements such as IGBTs and diodes are taken from their datasheets. In the first step the load of the simulated converter is a power variable load in a fixed DC voltage. Therefore the output DC current drawn from the converter is variable. Output current steps down from 95A in 5A steps during the simulation. In order to apply EPDC strategy [18], in the light load currents (less than 20A) only two phases of the lower stage will conduct the current. When the load current is higher than 20A and lower than 30A, one additional phase from the upper stage (conventional stage) starts conducting. For load current higher than 30 A, all four phases participate in load supplying.

The RMS currents of the four switches in full loading range are shown in Fig. 4. As it can be seen, below the 20A only two phases are conducting and only S3 and S4

switches are switched. The load current is splitted equally between these two legs. When the load current increases from 20A, since S2 conducts the current, the current passing through S3 and S4 decreases. When all four switches conduct the current, the current passing into switches S1 and S2 is equal.

As mentioned before, the input current ripple of the converter is an important issue that should be investigated. The proposed converter consists of two stages which its upper stage is a conventional two-leg interleaved converter. The duty cycles of the upper stage switches are also different from the duty cycles of the lower stage ones. Therefore, the current ripples of these two stages are calculated separately. In order to calculate the current ripple of each stage, only interval 1 of Fig.3 should be considered. Since in this interval, all inductors are in charging mode and therefore their current are rising, the maximum peak-to-peak input current ripple of each stage happens in interval 1. Therefore, the input current ripple reaches its maximum peak-to-peak value in this interval. The time duration of interval 1 is calculated as follows.

$$\Delta t_1 = \left(\frac{T_s}{2} - D_1 T_s \right) \quad (10)$$

Using (10), the maximum ripple of the current passing through inductor L1 and L2 can be calculated as:

$$\Delta i_{1,2} = \Delta i_{L_1} + \Delta i_{L_2} = \Delta t_1 \left(\frac{V_{in}}{L_1} + \frac{V_{in}}{L_2} \right) \quad (11)$$

where $L_1=L_2$. By using (1) and after some simplifications, the following equation is derived for the upper stage current ripple.

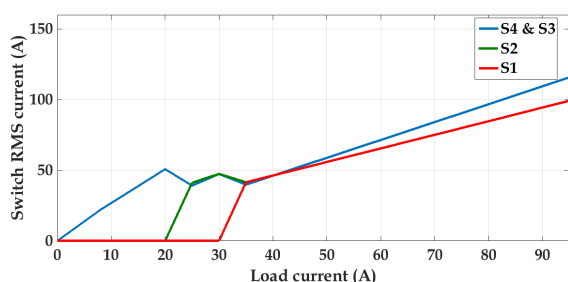


Fig. 4. RMS current of switches versus load current

$$\Delta i_{1,2} = \frac{T_s V_{in}}{L_1} (2D_1 - 1) = \frac{T_s V_o}{L_1} (2D_1 - 1) (1 - D_1) = \frac{T_s V_o D'_1}{L_1} (2D_1 - 1) \quad (12)$$

Same as the upper stage and by using (3), the current ripple of the lower stage is calculated as (13) and (14).

$$\Delta i_{3,4} = \Delta i_1 \left(\frac{V_{in}}{L_3} + \frac{V_{in}}{L_4} \right) \quad (13)$$

$$\Delta i_{3,4} = \frac{T_s V_{in}}{L_3} (2D_2 - 1) = \frac{T_s V_o}{2L_3} (2D_2 - 1) (1 - D_2) = \frac{T_s V_o D'_2}{2L_3} (2D_2 - 1) \quad (14)$$

Input current of the converter is depicted in Fig. 5(a). The current waveforms of Inductors 1 and 2 and the upper stage - the summation of the mentioned inductors current - are shown in Fig. 5(b) and Fig. 5(c), respectively. Furthermore, the current waveforms of inductors 3 and 4 and the input current of the lower are illustrated in Fig. 5(a) and Fig. 5(e), respectively. All current waveforms are normalized by full-load current. As it is seen from Fig. 5(a), the ripple of the total input current of the proposed converter is about 4% in full load operation. The upper stage current ripple is about 5% and the lower stage peak-to-peak current ripple is about 1% of the nominal value. By adjusting the phase shift in the switching pattern, total ripple of the converter input current equals the difference between the upper and lower stage current ripples.

For the voltage conversion ratio used in the simulation (144V/650V), according to (4), the switches of the lower stage possess a lower duty cycle. Therefore, their conduction losses are lower than the upstage switches. When the converter operates with open-loop and fixed output and

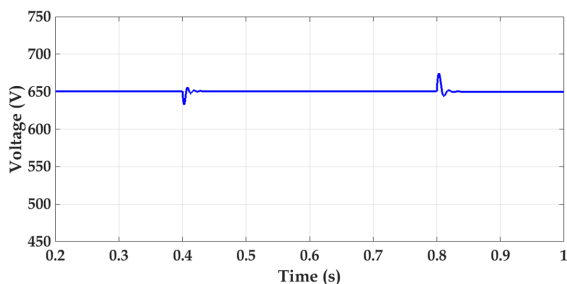


Fig. 6. Open-loop behavior of the output voltage during load current changes.

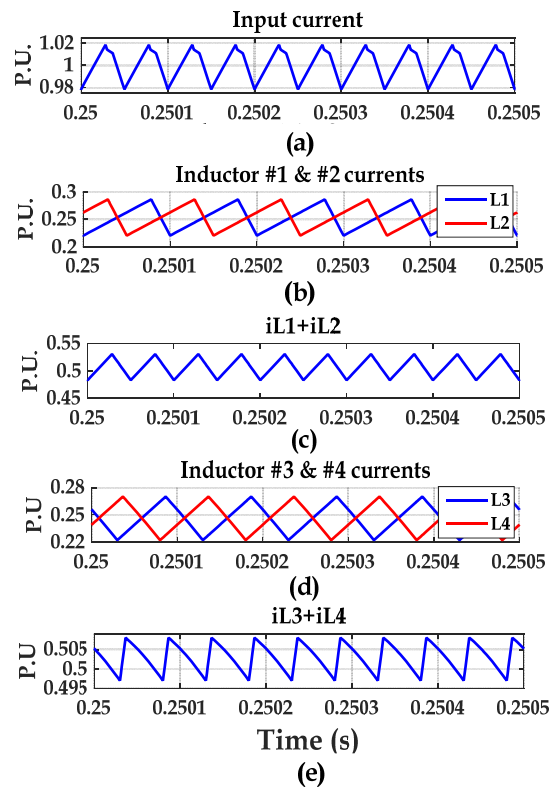


Fig. 5. Input and inductors per unit currents. (a) Converter input current. (b) Upper stage inductors currents. (c) Sum of upper stage currents. (d) Lower stage inductors currents. (e) Sum of lower stage currents.

input voltages, using (1) and (3) one can obtain D_1 and D_2 equal to 0.778 and 0.557 respectively.

Fig. 6 illustrates the output voltage of the converter in open-loop operation. The output current steps up from 15A to 25A at 0.45S and from 25A to 40A at 0.8S. It can be seen that the output voltage is fixed at 650V and the converter is stable. The closed-loop behavior of the proposed converter is also simulated. Fig.7 depicts control system of the proposed converter. Here, a simple PI controller is used to control the DC link voltage by adjusting the duty cycles of the switches. The EPDC unit generates the switch enable array to determine which switches should operate according to the demanded power.

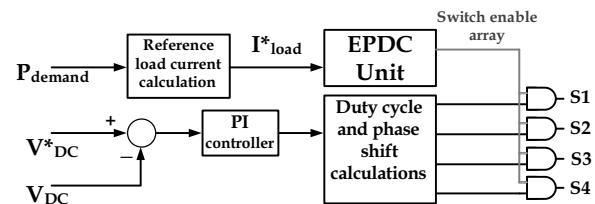


Fig. 7. Close-loop control system of the proposed converter

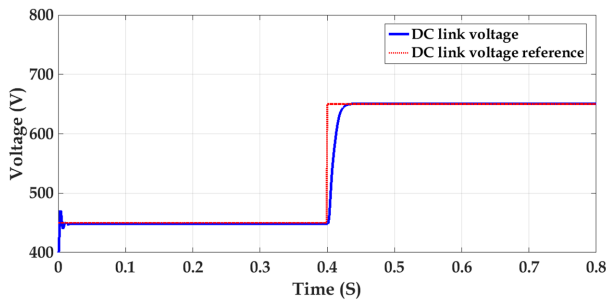


Fig. 8. Close-loop response of the output voltage to a step command

Response of the converter to a step change in output voltage from 450V to 650V is depicted in Fig.8. It is an important issue because in some cases the voltage of the DC link is not fixed [20]. It can be seen that the converter possesses a good response time (about 33ms).

Fig. 9 Shows a comparison between the power loss of the proposed converter and conventional converters during load current changes. The losses are calculated using (6) and (7). The proposed converter power dissipation is always less than the conventional ones, especially in light loads. The loss reduction in full load is about 12% but in light loads it reaches to about 40% compared with conventional converter with EPDC. The reasons for this loss reduction are the lower voltage rating of switches and lower duty cycles. The lower voltage rating of the switch, the lesser on-state resistance of the switch. Furthermore, lower duty cycle results in lower conduction loss. The loss reduction in light loads is more than heavy loads. In fact the operation of the proposed converter in light load conditions such as urban driving has a superb advantage over the conventional interleaved DC-DC converter.

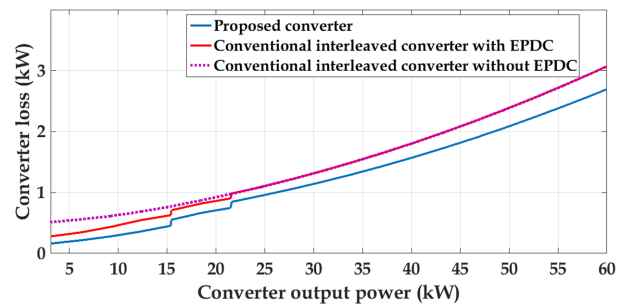


Fig. 9. Power dissipated by the proposed and conventional converters

3. 2. Simulation of the Proposed Converter Within an FCV

The proposed converter is suitable for an FCV. Therefore, the performance of this converter should be investigated and compared to a conventional interleaved boost converter in a vehicle simulator software. ADVISOR is used to simulate the FCV in driving cycles. Then, the power profile demanded from the FC in the driving cycles is extracted from the ADVISOR and is applied as the load of the converter. Finally the losses of the converter in those drive cycles are calculated using (6) and (7). Furthermore the conventional converter with EPDC is simulated in the same drive cycles too. After that, one can compare the losses of the two converters which operate in same the conditions and the same control strategy.

As an urban drive cycle, the UDDS drive cycle is selected to simulate the FCV. Fig. 10 shows the vehicle speeds versus operating time for this driving cycle. By simulating the FCV in the mentioned driving cycle, the power demanded from the FC stack is shown in Fig. 11. This power profile is divided into three sections. In high power demands (highlighted in red) all four phases of the converter conduct the current. In middle power range

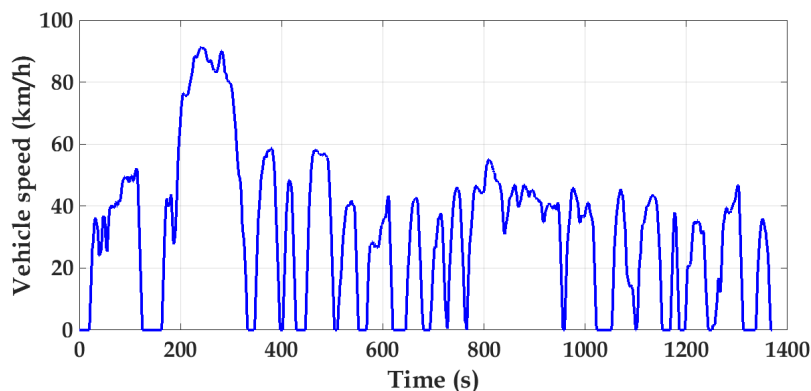


Fig. 10. Speed-time characteristic of UDDS drive cycle

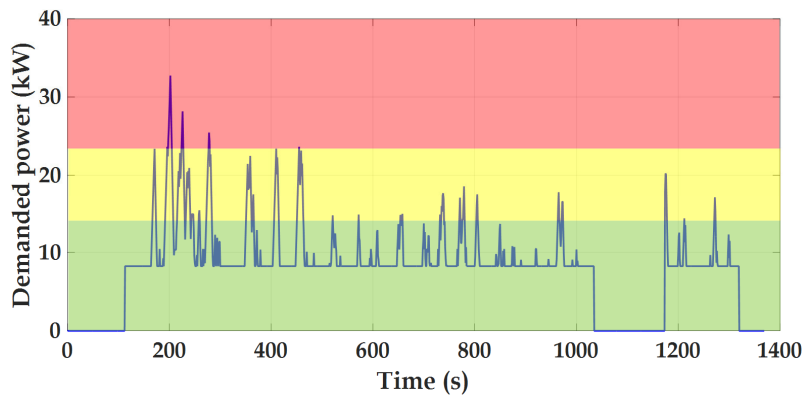


Fig. 11. FC output power in UDDS drive cycle

(highlighted in yellow), three phases participate in power supplying. In low output powers – which is most of the driving time in an urban driving cycle – only two phases of the converter, i.e., lower stage, is activated. This power section is highlighted in green in the power profile of Fig. 11.

By applying the power demand profile extracted from driving simulation to the proposed converter and conventional converter, the converter power loss profile of Fig. 12 is obtained using (6) and (7).

In this figure, the red curve is the power dissipated in conventional interleaved converter during the driving cycle versus time. The blue curve is the power loss of the proposed converter. Furthermore, the average power losses of the conventional and proposed converter are depicted. As it can be seen, the average power loss of the proposed converter in the simulated urban driving cycle is about 68% of the loss of the conventional converter. This is because of lower "off" state voltage of two switches of the proposed converter than conventional con-

verter switches. Furthermore, as mentioned before, the duty ratio of these two switches is also less than conventional one. Therefore, the conduction loss of the proposed converter is lower. Reducing the voltage stress of IGBTs may allow utilization of lower voltage rated IGBTs. Decreasing the voltage rating of the switches not only results into use of cheaper IGBTs, but also leads to smaller "on" state resistance i.e., lower r_c . Therefore, the conduction loss is further reduced.

A similar simulation and comparison are done in a highway drive cycle (US06_HWY) to investigate the performance of the proposed converter in a high power demand operation. Fig. 13 depicts the speed-time characteristics of this cycle. As it can be seen the vehicle speed is more than its speed in UDDS Urban driving cycle.

Fig.14 illustrates the FC output power in this drive cycle. As it can be seen the operation of the converter in the red zone is more than an urban drive cycle. It means that the converter operates for longer periods with four

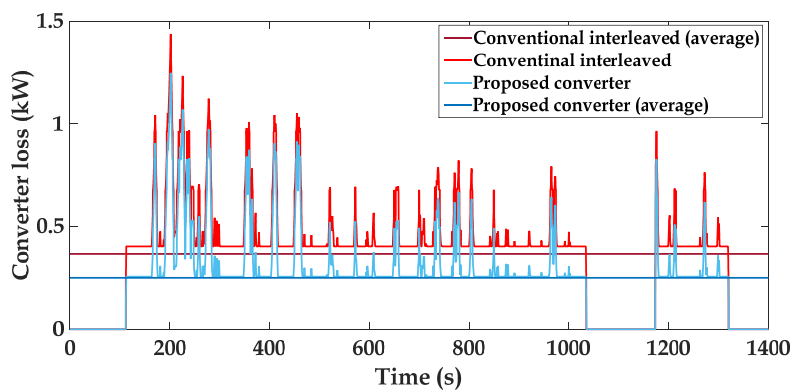


Fig. 12. Power losses of converters during UDDS cycle

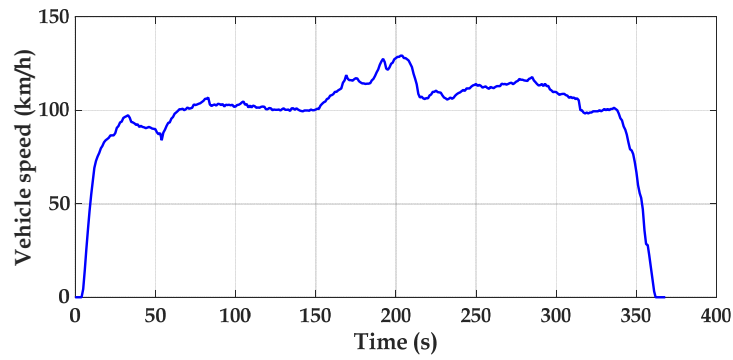


Fig. 13. Speed-time characteristic of US06_HWY

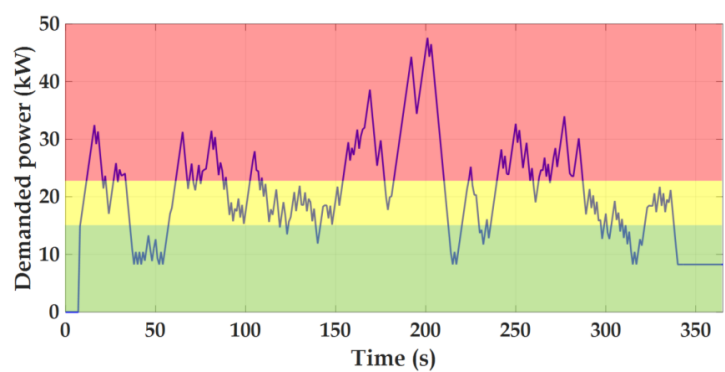


Fig. 14. FC output power in US06_HWY drive cycle

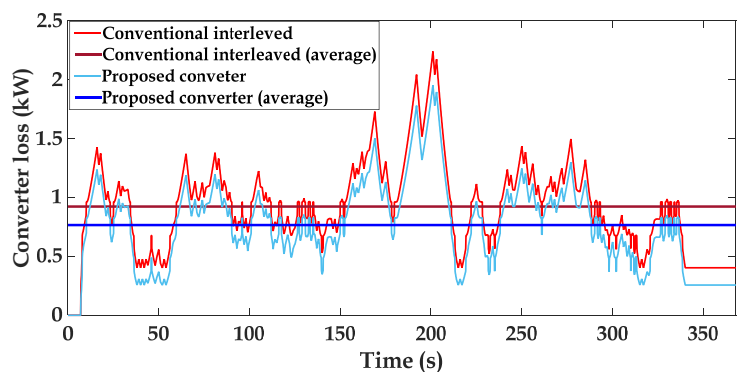


Fig. 15. Power losses of converters during US06_HWY cycle

legs. Fig. 15 depicts converter power losses when operating in this driving situation. It is seen that even in high power demand operation the proposed converter has less power dissipation compared to conventional one. The converter average loss is reduced to 83% of the conventional interleaved converter.

Fig. 16 summarizes the simulation results. As it is seen, in both driving cycles, i.e., urban and highway, the proposed converter possesses lower power loss. However

the difference between the average power losses in highway drive cycle is less than its counterpart in an urban drive cycle. This is because of this fact that as mentioned before, the proposed converter is more efficient in lighter load conditions. Because in light loads mostly two legs of the converter with lower voltage on their switches supply the power.

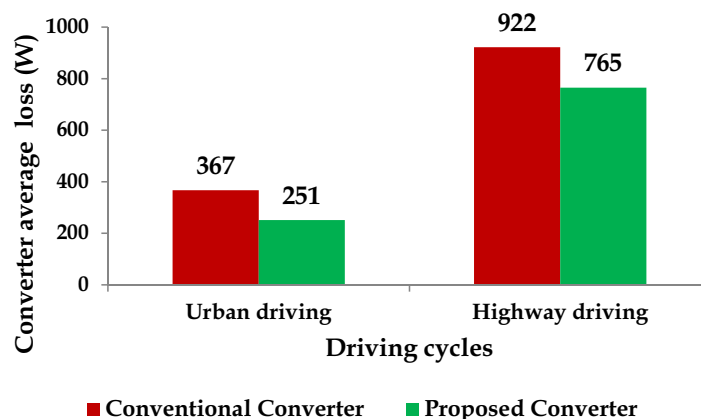


Fig. 16. Comparison of the converters power loss

4. Conclusion

In this paper, a novel DC-DC interleaved converter has been proposed. The steady-state characteristics of the converter were studied. Open-loop and close-loop behavior of the converter were investigated. Comparing to conventional interleaved converter, the proposed one has a lower switch voltage stress and lower duty cycle for its two switches. Therefore, the converter losses are reduced about 12% in full load and about 40% in light load conditions. Furthermore, the converter is simulated within an FCV by ADVISOR software in an urban and a highway drive cycles. In both drive cycles, the proposed converter seems more efficient than conventional interleaved converter which is used in existing FCVs such as TOYOTA MIRAI 2015. The results show that in urban drive cycle, the average losses of the converter are reduced about 32% compared to conventional converter. This reduction is about 17% in highway drive cycle. Therefore the proposed converter is more suitable for urban driving.

References

- [1] A. Emadi and S. S. Williamson, "Fuel cell vehicles: opportunities and challenges," in IEEE Power Engineering Society General Meeting, 2004., 2004, pp. 1640-1645 Vol.2.
- [2] A. Khaligh and Z. Li, "Battery, Ultracapacitor, Fuel Cell, and Hybrid Energy Storage Systems for Electric, Hybrid Electric, Fuel Cell, and Plug-In Hybrid Electric Vehicles: State of the Art," IEEE Transactions on Vehicular Technology, vol. 59, pp. 2806-2814, 2010.
- [3] C. Rayment and S. Sherwin, "Introduction to fuel cell technology," Department of Aerospace and Mechanical Engineering, University of Notre Dame, Notre Dame, IN, vol. 46556, pp. 11-12, 2003.
- [4] O. Hegazy, J. Van Mierlo, and P. Lataire, "Analysis, modeling, and implementation of a multidevice interleaved DC/DC converter for fuel cell hybrid electric vehicles," IEEE transactions on power electronics, vol. 27, pp. 4445-4458, 2012.
- [5] J. Bauman and M. Kazerani, "A comparative study of fuel-cell-battery, fuel-cell-ultracapacitor, and fuel-cell-battery-ultracapacitor vehicles," IEEE Transactions on Vehicular Technology, vol. 57, pp. 760-769, 2008.
- [6] A. Emadi, K. Rajashekara, S. S. Williamson, and S. M. Lukic, "Topological overview of hybrid electric and fuel cell vehicular power system architectures and configurations," IEEE Transactions on Vehicular Technology, vol. 54, pp. 763-770, 2005.
- [7] W. Li, Y. Zhao, J. Wu, and X. He, "Interleaved high step-up converter with winding-cross-coupled inductors and voltage multiplier cells," IEEE transactions on power electronics, vol. 27, pp. 133-143, 2012.
- [8] M. Khalilzadeh and K. Abbaszadeh, "Non-isolated high step-up DC-DC converter based on coupled inductor with reduced voltage stress," IET Power Electronics, vol. 8, pp. 2184-2194, 2015.
- [9] M. Khalilzadeh, M. Mahdipour, and K. Abbaszadeh, "High step-up DC-DC converter based on three-winding coupled inductor," in Power Electronics, Drives Systems & Technologies Conference (PEDSTC), 2015 6th, 2015, pp. 195-200.
- [10] C. M. Lai, C. T. Pan, and M. C. Cheng, "High-efficiency modular high step-up interleaved boost converter for DC-microgrid applications," IEEE Transactions on Industry Applications, vol. 48, pp. 161-171, 2012.
- [11] R. Ling, G. Zhao, and Q. Huang, "High step-up interleaved boost converter with low switch voltage stress," Electric Power Systems Research, vol. 128, pp. 11-18, 2015.
- [12] K. C. Tseng, J. T. Lin, and C. C. Huang, "High step-up converter with three-winding coupled inductor for fuel cell energy source applications," IEEE

Transactions on Power Electronics, vol. 30, pp. 574-581, 2015.

- [13] B. Wahdame, L. Girardot, D. Hissel, F. Harel, X. François, D. Candusso, et al., "Impact of power converter current ripple on the durability of a fuel cell stack," in Industrial Electronics, 2008. ISIE 2008. IEEE International Symposium on, 2008, pp. 1495-1500.
- [14] W. Choi, P. Enjeti, J. W. Howze, and G. Joung, "An experimental evaluation of the effects of ripple current generated by the power conditioning stage on a proton exchange membrane fuel cell stack," Journal of materials engineering and performance, vol. 13, pp. 257-264, 2004.
- [15] M. Khalilzadeh and A. Fereidunian, "A Markovian approach applied to reliability modeling of bidirectional DC-DC converters used in PHEVs and smart grids," Iranian Journal of Electrical & Electronic Engineering, vol. 12, pp. 0-0, 2016.
- [16] M. Nikzad and A. Radan, "Accurate loss modelling of fuel cell boost converter and traction inverter for efficiency calculation in fuel cell-battery hybrid vehicles," in Power Electronic & Drive Systems & Technologies Conference (PEDSTC), 2010 1st, 2010, pp. 218-223.
- [17] D. Graovac, M. Pürschel, "IGBT Power Losses Calculation Using the Data-Sheet Parameters", Infineon Application Note, V 1. 1, January 2009.
- [18] Y. Hasuka, H. Sekine, K. Katano, and Y. Nonobe, "Development of Boost Converter for MIRAI," SAE Technical Paper 0148-7191, 2015.
- [19] M. Ehsani, Y. Gao, and A. Emadi, "Modern electric, hybrid electric", and fuel cell vehicles: fundamentals, theory, and design: CRC press, 2009.
- [20] T. Schoenen, M. S. Kunter, M. D. Hennen, and R. W. De Doncker, "Advantages of a variable dc-link voltage by using a dc-dc converter in hybrid-electric vehicles," in Vehicle Power and Propulsion Conference (VPPC), 2010 IEEE, 2010, pp. 1-5.



Mohammad Khalilzadeh is a PhD Student in the University of Tehran, Tehran, Iran. He received his M.Sc. and B.Sc. in Electrical Engineering from K. N. Toosi University of Technology and the University of Tehran in 2012 and 2014 respectively. His research interests include power electronic converters, reliability in power electronics, renewable energy, and electric motor drives.



Mohammad Reza Nikzad received the B.Sc and M.Sc degrees from K. N. Toosi university of Technology both in power electrical engineering, in 2005 and 2008. Since 2011, he is pursuing his Ph.D. degree at University of Tehran, Tehran, Iran. His main research interests are in the areas of Electric, Electric Hybrid, and fuel cell vehicles, Power electronic converters Topology and Control, Power electronic converters Loss modeling, Electric motor drives, Battery and ultracapacitor energy storages and Soft switching techniques.



Behzad Asaei received his B.Sc. and M.Sc. degrees from the University of Tehran in 1988 and 1990, respectively, and his Ph.D. degree from the Sydney University in 1995, all in electrical engineering. From 1996 to 2006, he was with the Irankhodro Company Research and Development Center as Electrical Engineer Design Manager and doing research in automotive industry mainly on solar, electric and hybrid electric vehicles, while simultaneously he has been at the University of Yazd as Assistant professor. Since 2006, he has been at the University of Tehran, school of Electrical and Computer Engineering, where he is an associate Professor and director of the Energy and Automotive Technology Lab. He was the vice president of the Mapfan Research Institute a joint institute between the University of Tehran and Mapna Group that is doing research in the fields of power generation, rail industry, and oil and gas industry from 2010 to 2014. Since 1996, he was Managing director of several companies in the field of Automotive, and Energy Sectors. From 2014 he joined Mah-Taab group as Managing Director of Arian Mah-Baad Company that is an IPP in the field of renewable energy in several wind farms that are under construction and development with 3.2 and 3.4 MW Siemens PMDD Wind turbines. His research is focused in the field of automotive electronics, wind energy, solar energy, solar, electric and hybrid electric vehicles, power electronics, motor drives, and power generation in which several projects are completed.